BELLCOMM, INC.
1100 SEVENTEENTH STREET, N.W. WASHINGTON, D.C. 20036

COVER SHEET FOR TECHNICAL MEMORANDUM

TITLE- Semi-Analytic Solution to an Optimum, Two-Impulse Targeting Problem

TM- 68-2011-1

DATE- March 7, 1968

FILING CASE NO(S)- 310

AUTHOR(S)- S. L. Levie, Jr.

FILING SUBJECT(S)- (ASSIGNED BY AUTHOR(S)-
Targeting
Lunar Deboost
Two-Impulse Deboost
Multiple Impulse Deboost
Accessibility

ABSTRACT

A two-impulse model for deboost into lunar orbit has been developed analytically, optimized, and incorporated into the Bellcomm Apollo Simulation Program. The model considered restricts the trajectory between the two impulses to be circular.

This paper presents the analysis of the two-impulse model and includes closed-form expressions for the ΔV for both a one- and a two-impulse deboost. It also compares these two modes of deboost, obtaining two principal results: (1) the two-impulse deboost increases the accessible lunar surface area; (2) the two-impulse deboost can provide fuel savings of about 300 pounds for selected, low-latitude sites on selected launch dates.

MAR 1968
RECEIVED

(NASA-CR-93606) SEMI-ANALYTIC SOLUTION TO AN OPTIMUM, TWO-IMPULSE TARGETING PROBLEM (Bellcomm, Inc.) 47 p

N79-71855

Unclas
00/13 11128

FF No. 602(A)
(PAGES) (CODE)
CR#93606
(NASA CR OR TMX OR AD NUMBER) (CATEGORY)
[redacted]

BA-145A (3-67)

SEE REVERSE SIDE FOR DISTRIBUTION LIST

TABLE OF CONTENTS

		Page
1.0	INTRODUCTION	1
2.0	THE TWO-BURN DELTA VELOCITY	3
2.1	Geometry	3
2.2	Delta Velocity at the Second Burn	5
2.3	Delta Velocity at the First Burn	7
2.4	Optimization of the Two-Burn Delta Velocity	11
2.5	Reduction to the One-Burn Case	13
3.0	RESULTS OF TWO-BURN SIMULATIONS	17
3.1	Accessibility Filaments	17
3.2	Data for Selected Sites	27
4.0	SUMMARY AND CONCLUSIONS	28
ACKNOWLEDGEMENTS		30
REFERENCES		31
APPENDIX I:	Some Properties of a Hyperbola	32
APPENDIX II:	The T_1 Optimization	35
II.1	Choice of D	35
II.2	Optimization with Respect to T_1	36
II.3	Example Solution	39

LIST OF TABLES

Table		Page
3.1	Data for Accessibility Filaments at 1.0° West Longitude for Launch Date October 29, 1968 (Lunar Module Plane Change)	22
3.2	Data for Accessibility Filaments at 1.0° West longitude for Launch Date October 29, 1968 (Command Module Plane Change)	23
3.3	Data for Accessibility Filaments at 30.0° West Longitude for Launch Date October 29, 1968 (Command Module Plane Change)	24
3.4	Comparison of One- and Two-Burn Missions to Several Orbiter Sites	25

LIST OF ILLUSTRATIONS

Figure		Page
2.1	The Two-Burn Geometry	6
2.2	Spherical Projection Showing Two-Burn Geometrical Quantities	6
2.3	Velocity Vector Diagram at Point of First Transfer	9
3.1	Accessibility Filaments at 1.0° West Longitude for Launch Date October 29, 1968 (Lunar Module Plane Change)	19
3.2	Accessibility Filaments at 1.0° West Longitude for Launch Dage October 29, 1968 (Command Module Plane Change)	20
3.3	Accessibility Filaments at 30.0° West Longitude for Launch Date October 29, 1968 (Command Module Plane Change)	21
II.1	Choosing D	35
II.2	Choosing D	36
II.3	Computation of H, H^2, and $(1+\tan^2 T_1)H^2$	37
II.4	Computation of N, N^2, and the tan T_1 Polynomial	37
II.5	Plot of ΔV_{2B} vs T_1	38

BELLCOMM, INC.
1100 Seventeenth Street, N.W. Washington, D.C. 20036

SUBJECT: Semi-Analytic Solution to an Optimum, Two-Impulse Targeting Problem - Case 310

DATE: March 7, 1968

FROM: S. L. Levie, Jr.

TM-68-2011-1

TECHNICAL MEMORANDUM

1.0 INTRODUCTION

In recent years there has been increasing interest in multiple-impulse deboosts into lunar parking orbit. This subject has been explored in two prior Ballcomm studies, both concerning themselves with two-impulse deboosts.

The first investigation, by P. Gunther (Reference 1), was an analytical optimization study which permitted changing the orientation and the dynamic properties of the approach hyperbola at the moon's sphere of influence, coasting on the new trajectory until intersection with the desired lunar parking orbit, and then making a one-impulse deboost into this parking orbit. This attractive model has not been applied to targeting in the Apollo program.

The second study, by J. S. Dudek (References 2, 3), treated a model much more restrictive than Gunther's, in that the intermediate trajectory is forced to be circular and of the same radius as the desired parking orbit. Optimized parametrically, this model does increase the area of the lunar surface which is accessible over that accessible through the use of only a single-impulse deboost.

In the present study, Dudek's model is treated analytically,* allowing more insight into the mechanics of the problem. The analysis is presented in Section 2.0. Furthermore, the analytic model has been built into the Ballcomm Apollo Simulation Program (BCMASP), making it possible to simulate in the

---

*It must be mentioned that Dudek placed on his model a restriction which is not made in this paper, namely, that the coast arc in the intermediate circular orbit be ninety degrees. A result of the present study is that the coast arc is actually variable from mission to mission.

patched conic domain those lunar missions which deboost with two impulses into lunar orbit from free-return hyperbolas. The modified version of BCMASP, called DBST, is described in detail in a companion memorandum to be published soon.

The two-impulse model is put into perspective as a possible strategy for Apollo in Section 3.0. It should be noted that the results of this section are provided primarily to illustrate and verify the analysis and implementation of the two-impulse model. Beyond this the results must be regarded as only indicative of what one might expect from a comprehensive study employing the two-impulse strategy.

As a final note, the expressions "two-burn model" and "two-burn deboost" will appear frequently in the text. They should always be regarded as referring to the analytic model described above (with no restriction on the coast arc). Similar expressions using "one-burn" will refer to Apollo's present mode of deboosting into lunar parking orbit.

2.0 THE TWO-BURN DELTA VELOCITY

If a certain velocity increment is required in a maneuver, its magnitude may be expressed as an equivalent fuel weight requirement. Since velocity changes are closer to the kinematics of a problem than are fuel weights, one ordinarily computes the magnitude of the velocity increment, calling this the characteristic delta velocity of the maneuver. For a sequence of maneuvers in which there is no vehicle staging, the total delta velocity requirement is the sum of the delta velocities at each maneuver.

The delta velocity will be computed for a sequence of two impulsive maneuvers, the first of which carries a mass from an arbitrary hyperbola* to an intermediate circular orbit about the attracting body, and the second of which carries the mass from this orbit to a final circular orbit of equal radius. The net effect may be described as a two-burn maneuver, since in practice a rocket must be ignited at each of the two orbit transfers. If the orientation of the final circular orbit is specified, then all geometrical properties can be measured relative to its plane. This will be done in what follows.

In addition to computing the two-burn delta velocity, its optimization will also be investigated, in order to determine when the optimum two-burn deboost reduces to the one burn case.

It should be borne in mind that because they deal only with velocity magnitudes, the principal results of this section apply as well to the inverse problem, which is a two-burn boost out of an initial circular orbit.

2.1 Geometry

Let the inclination of the plane of the hyperbola be called P. P is also the included angle between the angular momentum vectors of the orbit and the hyperbolic orbit. It may range between 0° and 180°.

To specify the orientation of the hyperbola in its plane, one must specify F, the true anomaly of the node line. This is a signed quantity, and the sign convention is established by fixing the direction of increasing true anomaly as the direction

---

*To have impulsive maneuvers, the hyperbola obviously must have a pericenter distance which is less than or equal to the circle's radius. This condition is assumed for this paper. Beyond this, however, the hyperbola's dynamic and orientation parameters may be arbitrary.

of motion along the hyperbola. Thus F is positive if the node line is crossed after pericenter and negative if the node line is crossed before pericenter. Without loss of generality the distinction between ascending and descending node may be ignored, allowing F to be measured in such a way that $|F| \leq 90°$.

Suppose the final circular orbit has a radius R_c. If the hyperbola's pericenter is a distance R_p from the attractive center then the maneuvering sequence requires the condition $R_p \leq R_c$. If $R_p < R_c$ there will be just two points on the hyperbola at which transfer to the intermediate circular orbit can be effected. Denoting the true anomaly of one of these points by ϕ, it can be shown for a hyperbolic trajectory* that

$$\cos\phi = \frac{p/R_c - 1}{p/R_p - 1} \quad , \tag{2.1}$$

where p, the parameter of the hyperbola, may be written*

$$p = 2R_p\left(\frac{ER_p}{GM} + 1\right) \tag{2.2}$$

E is the hyperbolic energy, and GM is the gravitational constant times the mass of the attracting body. Since the cosine function is even, ϕ has an ambigous sign:

$$\left.\begin{aligned} \phi &= D \arccos\left(\frac{p/R_c - 1}{p/R_p - 1}\right) \\ D &= \begin{cases} +1 \text{ if transfer is after pericenter} \\ -1 \text{ if transfer is before pericenter.} \end{cases} \end{aligned}\right\} \tag{2.3}$$

With this definition of D, F and ϕ have the same sign convention. The extremum values of ϕ are $\pm$ 180°.

---

*See Appendix I.

Further quantities which must be defined are $N_1 \equiv F - \phi$, the (signed) angle* from the first transfer point to the node line; T_1, the (signed) angle between the planes of the hyperbola and the intermediate circle; and T_2, the angle between the planes of the intermediate and final circles. T_1 is considered positive if $\vec{V}_I \times \vec{V}_H$ is parallel to the radius vector to the transfer point, where $\vec{V}_I$ is the velocity on the intermediate circle and $\vec{V}_H$ is the horizontal component of the hyperbolic velocity. T_1 is chosen so as to lie in the range $-180° < T_1 \leq 180°$.

These geometrical quantities are shown with positive senses in a three dimensional drawing in Figure 2.1 and in a spherical projection in Figure 2.2. Also shown are C, the angle between the two transfer points, and N_2, the angle between the node and the second transfer point.

With the geometry established, the total two-burn delta velocity, ΔV_{2B}, may now be computed. ΔV_{2B} is the sum of the delta velocities at the first and second transfers.

2.2 Delta Velocity at the Second Burn

It is desired to compute $\Delta V_2 = |\Delta\vec{V}_2|$, where $\Delta\vec{V}_2$ is the delta velocity vector which takes the mass from the intermediate circular orbit, with velocity $\vec{V}_i$, to the final circular orbit, with velocity $\vec{V}_f$. The vector addition is illustrated at the right. Notice that both $\vec{V}_i$ and $\vec{V}_f$ are perpendicular to the radius vector to Z, the second transfer point. Since $|\vec{V}_i| = |\vec{V}_f| \equiv V_c$,

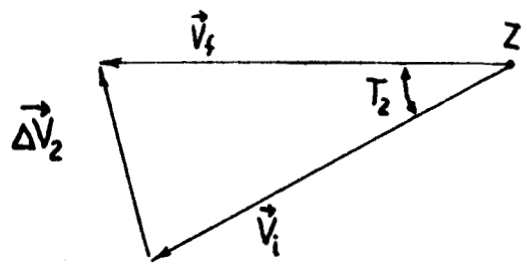

$$\Delta V^2 = 2V_c \sin\frac{T_2}{2} = 2V_c\sqrt{\frac{1 - \cos T_2}{2}} \qquad (1.4)$$

*The sign convention is the same as for F.

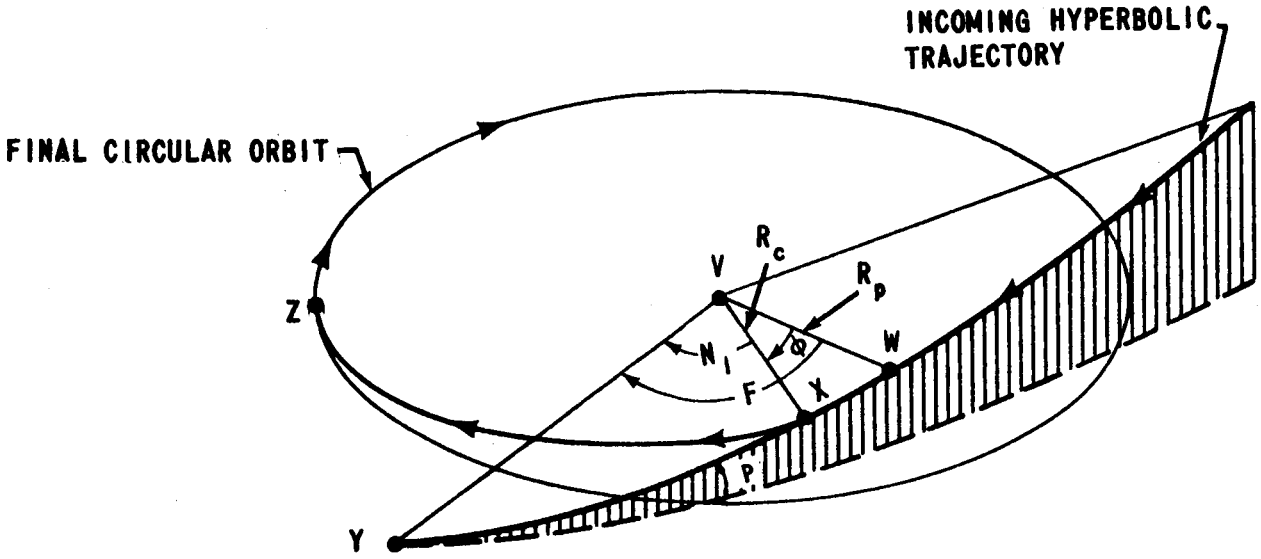

FIGURE 2.1 - THE TWO-BURN GEOMETRY

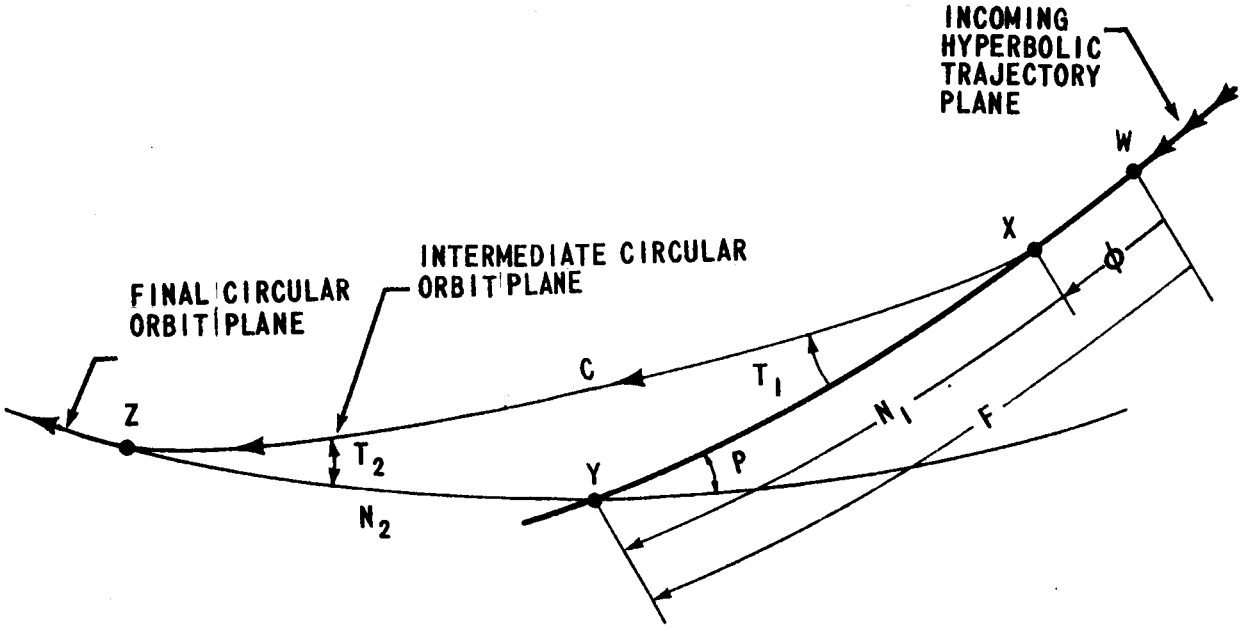

FIGURE 2.2 - SPHERICAL PROJECTION SHOWING TWO-BURN GEOMETRICAL QUANTITIES

KEY:

V-CENTER OF ATTRACTION
W-PERICENTER
X-POINT OF FIRST TRANSFER
Y-NODE
Z-POINT OF SECOND TRANSFER

Using the spherical trigonometric "cosine law for angles" on the spherical triangle below,

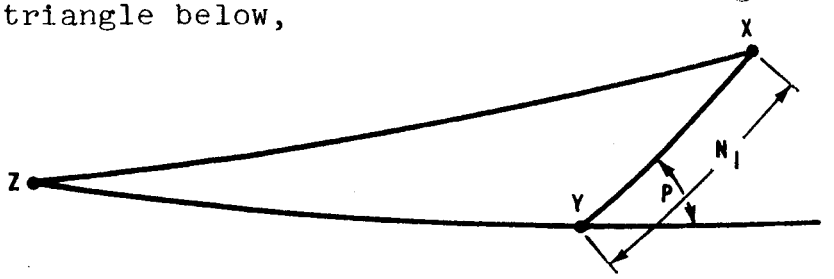

$$\cos T_2 = \cos T_1 \cos(\pi - P) + \sin T_1 \sin(\pi - P) \cos N_1$$

$$= \cos T_1 \cos P + \sin T_1 \sin P \cos N_1$$

This result also holds if X, the first transfer point, is below the reference plane. Hence, for the general case,

$$\Delta V_2 = \sqrt{2} V_c \sqrt{1 - \cos T_1 \cos P - \sin T_1 \sin P \cos N_1}$$

Inserting N_1, ϕ, and $V_c = \sqrt{\frac{GM}{R_c}}$ gives

$$\Delta V_2 = \sqrt{\frac{2GM}{R_c}} \left[1 - \cos T_1 \cos P - \sin T_1 \sin P \cos F - D \cos^{-1}\left(\frac{\frac{p}{R_c} - 1}{\frac{p}{R_p} - 1} \right) \right]^{\frac{1}{2}} \tag{2.5}$$

in which D is defined in Equation (2.3).

2.3 Delta Velocity at the First Burn

The computation of $\Delta V_1 = |\Delta \vec{V}_1|$, the delta velocity which takes the mass from the hyperbola to the intermediate circle, is more complicated, since the vector increment $\Delta \vec{V}_1$ must

(i) reduce the flight path angle to zero

(ii) obtain circular velocity $|\vec{V}_c|$

(iii) finally, yaw through an angle T_1 to obtain the intermediate circular velocity $\vec{V}_i$.

This may be achieved by (i) removing the entire radial component, $\vec{V}_{RH}$, of the hyperbolic velocity; (ii) adding to the horizontal component, $\vec{V}_H$, of the hyperbolic velocity an increment $\Delta\vec{V}_H = -\vec{V}_H + \vec{V}_c$; and (iii) adding to the instantaneous circular velocity an out-of-plane increment $\Delta\vec{V}_c$ of magnitude $2V_c \sin\frac{T_1}{2}$ These vector increments are illustrated in Figure 2.3. Thus the net increment is

$$\Delta\vec{V}_1 = \Delta\vec{V}_c + \Delta\vec{V}_H - \vec{V}_{RH}$$

In this formula, the first two vectors are perpendicular to $\vec{R}_c$, and $\vec{V}_{RH}$ is parallel to it. Looking anti-parallel to $\vec{R}_c$ we see the vectors at the right (compare with Figure 2.3), for which it is readily shown that $\gamma = \frac{1}{2}(\pi + T_1)$. Using this and the cosine law for plane triangles gives

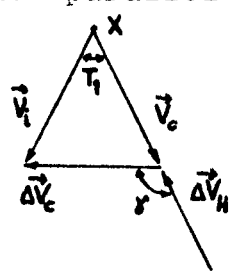

$$|\Delta\vec{V}_c + \Delta\vec{V}_H| = \left(\Delta V_c^2 + \Delta V_H^2 - 2\Delta V_c\ \Delta V_H \cos\gamma\right)^{\frac{1}{2}}$$

$$= \left(\Delta V_c^2 + \Delta V_H^2 + 2\Delta V_c\ \Delta V_H \sin\frac{T_1}{2}\right)^{\frac{1}{2}}.$$

Since $\vec{V}_{RH}$ is perpendicular to the plane of $\Delta\vec{V}_c$ and $\Delta\vec{V}_H$, it is also perpendicular to $\Delta\vec{V}_c + \Delta\vec{V}_H$, so we may use Pythagoras' theorem to obtain ΔV_1:

$$\Delta V_1^2 = |\Delta\vec{V}_c + \Delta\vec{V}_{\theta H}|^2 + V_{RH}^2$$

$$= V_{RH}^2 + \Delta V_c^2 + \Delta V_{\theta H}^2 + 2\Delta V_c\ \Delta V_{\theta H} \sin\left(\frac{T_1}{2}\right).$$

The expression for V_{RH}, ΔV_c, and ΔV_H will now be computed.

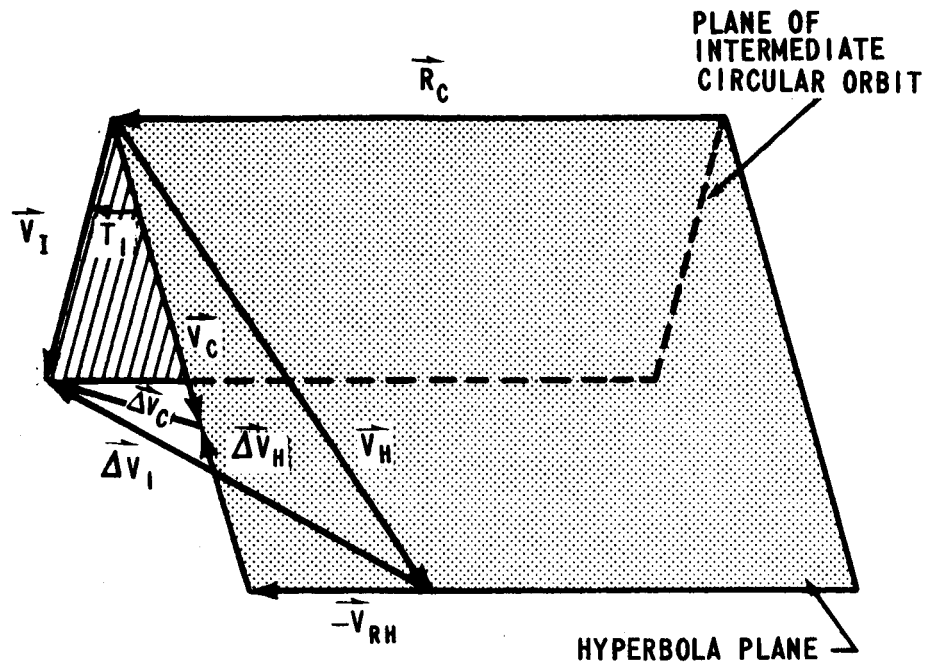

TRANSFERRING FROM THE HYPERBOLA (VELOCITY V_H) TO THE INTERMEDIATE CIRCULAR ORBIT (VELOCITY V_I) MAY BE VIEWED AS CONSISTING OF THREE, SIMULTANEOUS STEPS:

(I) REMOVE FLIGHT PATH ANGLE OF HYPERBOLIC TRAJECTORY ($-\vec{V}_{RH}$)

(II) OBTAIN INSTANTANEOUS CIRCULAR VELOCITY $\vec{V}_C$ IN HYPERBOLA PLANE ($\Delta\vec{V}_H$))

(III) YAW $\vec{V}_C$ THROUGH ANGLE T_I TO OBTAIN THE INTERMEDIATE CIRCULAR VELOCITY $\vec{V}_I$ ($\Delta\vec{V}_C$).

THE TOTAL DELTA VELOCITY REQUIRED IS:

$$\Delta\vec{V}_I = -\vec{V}_{RH} + \Delta\vec{V}_H + \Delta\vec{V}_C$$

FIGURE 2.3 - VELOCITY VECTOR DIAGRAM AT POINT OF FIRST TRANSFER

It can be shown that

$$V_{RH}^2 = V_c^2 \left(2 + \frac{2ER_c}{GM} - \frac{p}{R_c}\right)$$

At the beginning of this section it was pointed out that

$$V_c = 2V_c \sin \frac{T_1}{2} \quad ,$$

and at the same time it was stated that $\Delta\vec{V}_H = -\vec{V}_H + \vec{V}_c$. Since $\vec{V}_{\theta H}$ and $\vec{V}_c$ are parallel, then $|\Delta\vec{V}_H| = V_H - V_c$. But*

$$V_H = V_c\sqrt{\frac{p}{R_c}} \quad ,$$

whence

$$\Delta V_H = V_c\left(\sqrt{\frac{p}{R_c}} - 1\right) \quad .$$

Making the necessary substitutions into ΔV_1^2 yields the result

$$\Delta V_1^2 = V_c^2 \left(3 + \frac{2ER_c}{GM} - 2\sqrt{\frac{p}{R_c}} \cos T_1\right) \quad .$$

Finally, combining ΔV_1 and ΔV_2, the two-burn delta velocity becomes

$$\Delta V_{2B} = \sqrt{\frac{2GM}{R_c}}\left\{\left(\frac{3}{2} + \frac{ER_c}{GM} - \sqrt{\frac{p}{R_c}} \cos T_1\right)^{\frac{1}{2}} + \left(1-\cos T_1 \cos P - \sin T_1 \sin P \cos\left[F - D\cos^{-1}\left(\frac{p/R_c - 1}{p/R_p - 1}\right)\right]\right)^{\frac{1}{2}}\right\} \tag{2.6}$$

*See Appendix I.

where D is defined to be

$$D = \begin{cases} +1 \text{ if the first burn is after pericenter} \\ -1 \text{ if the first burn is before pericenter.} \end{cases}$$

2.4 Optimization of the Two-Burn Delta Velocity

It is of great interest to determine what set of parameter values minimizes ΔV_{2B}. Close scrutiny of Equations (2.6) and (2.2) shows that an effort to make definite statements about the overall optimization of ΔV_{2B} is probably futile, due to the complicated, non-linear relations between the parameters, which are observed to be E, R_c, P, F, T_1 and R_p.* One must instead see what may be said with particular applications in mind. Therefore, a specialized context, that of free-return Apollo missions with two-burn deboosts into lunar orbit, will now be assumed.

In this context, the only parameter which becomes a fixed number is the lunar parking orbit radius, R_c. This is fixed by program specifications. In addition, the free-return constraint has the effect of restricting both P and E to definite but unknown ranges. Not knowing how to compute these ranges, both P and E will be regarded as given anticipating that their optimum values will be provided by the outer iteration loops of a trajectory targeting scheme. Finally, the angle F will be removed from the list of free parameters, because it is determined by P, R_p, and the hyperbola's velocity vector at infinity. The latter quantity will also be produced by the targeting scheme.

An accounting shows that in this context the remaining free parameters are the quantities T_1 and R_p. Thus, to optimize ΔV_{2B}, derivatives will be taken with respect to T_1 and R_p, set equal to zero, and the resulting equations solved simultaneously.

---

*The quantity D has been omitted from the list of arguments because its optimum value is readily determined once F is given. Under normal conditions, as explained in Appendix II, one should take D = sign(F). It will be assumed in the following that this choice has been made.

The differentiation by T_1 is extremely involved and is therefore presented as Appendix II. The simplified result is a sixth degree polynominal in tan T_1 (see Equation (II.10), on Figure II.4, Appendix II). If one is given R_p, this polynominal may be solved by numerical methods.

The numerical solutions are not always dependable, however, because for R_p such that N_1 is small ($N_1 \lesssim 0.1°$), the polynominal becomes ill-conditioned. In an operational sense this means that some roots are so nearly degenerate that they cannot be resolved with acceptable precision. It also means that obvious transformations and approximations in small quantities fail to produce acceptably precise roots.

In these nearly degenerate cases one is therefore reduced to iterating ΔV_{2B} as a function of T_1 in order to obtain the minimum. As shown in the next section, the optimum T_1 is only slightly less than P, for N_1 very small. This fact provides a very good starting point for the iteration, producing rapid convergence. Thus, if outside the region of small N_1 one solves the T_1 polynominal and inside that region iterates on T_1, excellent solutions can be obtained for <u>all</u> values of N_1.

The derivative of ΔV_{2B} by R_p is much more complicated than the derivative by T_1; it appears to lead to a twelfth degree polynominal. Since the two polynominals in T_1 and R_p would have to be solved iteratively to find the optimum point, the possibility of iterating without doing the R_p is attractive. This approach has been found to be successful, because T_1 is only weakly dependent on R_p. The iteration scheme adopted is:

(i) Choose $R_p = R_c$ initially.

(ii) For this R_p compute the optimum T_1.

(iii) In ΔV_{2B} insert the optimum T_1 and increment R_p until a minimizing value is found.

(iv) Return to step (ii) and continue looping until T_1 and R_p stabilize.

In practice the iteration loop needs to be executed only twice.

It may be observed that varying R_p is equivalent to varying N_1, the angle between the first burn point and the node line. It is important to keep this in mind when considering the geometry of the two-burn model.

2.5 Reduction to the One-Burn Case

Because the geometry of the two-burn problem contains the one-burn geometry as a subset, one should determine when the optimum two-burn maneuver will have in fact only one burn. It will be shown in this section that if the optimization of the two-burn geometry produces $N_1 = 0$ (the condition for the approach hyperbola to intercept the parking orbit) then the optimum two-burn deboost need not degenerate to a one-burn deboost, contrary to one's expectations. Stated differently, if the constraint $N_1 = 0$ is imposed on the deboost geometry, then a one-burn deboost is not necessarily optimum.

The two-burn problem obviously cannot degenerate unless the first burn occurs at the node line. This requires that R_p be adjusted such that N_1 is zero, or

$$N_1 = F - D \quad \arccos\left(\frac{p/R_c - 1}{p/R_p - 1}\right) = 0 \quad . \tag{2.7}$$

Inserting this into Equation (2.6) and recognizing that $\sqrt{GM/R_c}$ is the circular velocity V_c produces

$$\Delta V_{2B} = \sqrt{2}V_c\left\{\left(\frac{3}{2} + \frac{E}{V_c^{\,2}} - \sqrt{\frac{p}{R_c}}\cos T_1\right)^{\frac{1}{2}} + \left(1 - \cos(T_1 - P)\right)^{\frac{1}{2}}\right\} \tag{2.8}$$

Observe that if this is to produce the one-burn case, then the entire plane change must be made at the first burn, or $T_1 = P$. Making this substitution yields a <u>formula for the one-burn delta velocity</u>:

$$\Delta V_{1B} = \sqrt{2}V_c \left(\frac{3}{2} + \frac{E}{V_c^{\,2}} - \sqrt{\frac{p}{R_c}} \cos P\right)^{\frac{1}{2}} \quad . \tag{2.9}$$

Now consider Equation (2.8), which describes a two-burn deboost in the neighborhood of the one-burn solution. To do this, let T_1 be less than P by some amount θ: $T_1 = P - \theta$.* As a function of θ, then

$$\Delta V_{2B}(\theta) = \sqrt{2}V_c \left\{\left(\frac{3}{2} + \frac{E}{V_c^{\,2}} - \sqrt{\frac{p}{R_c}} \cos(P - \theta)\right)^{\frac{1}{2}} + (1 + \cos\theta)^{1/2}\right\} . \tag{2.10}$$

In order to introduce Equation (2.9) to this formula, add and subtract $\sqrt{p/R_c}$ cos P to the cos(P - θ) term of Equation (2.10), getting

$$\Delta V_{2B}(\theta) = \sqrt{2}V_c \left\{\left(\frac{\Delta V_{1B}^{\,2}}{2V_c^{\,2}} - 2\sqrt{\frac{p}{R_c}} \sin(P - \frac{\theta}{2}) \sin\theta/2\right)^{\frac{1}{2}} + \sqrt{2} \sin\theta/2\right\} \quad . \tag{2.11}$$

The trigonometric identities

$$\cos x - \cos y = -2 \sin\left(\frac{x + y}{2}\right) \sin\left(\frac{x - y}{2}\right)$$

---

*On physical grounds it is obvious that $\theta < 0$ need not be considered, since this would mean $T_1 = P + |\theta|$. The two-burn deboost can never be optimum in this case, because too much plane change would be made at the first burn, requiring the excess to be removed at the second burn. For the same reason $\theta > P$ need not be considered. Thus, the interesting values of T_1 lie in the range 0 to P.

and

$$\sqrt{1 - \cos x} = \sqrt{2} \sin \frac{x}{2}$$

have been used to obtain this expression.

Let θ approach an infinitesimal value ε. The aim is to expand $\Delta V_{2B}(\varepsilon)$ and keep only first order terms in ε. In the limit, the second term in the square root in Equation (2.11) becomes tiny, and only the first two terms of a binominal expansion of the radical need be used. This results in

$$\Delta V_{2B}(\varepsilon) = \Delta V_{1B} - \frac{2V_c}{\Delta V_{1B}} \sqrt{\frac{p}{R_c}} \sin\left(P - \frac{\varepsilon}{2}\right) \sin \frac{\varepsilon}{2}$$

$$+ \sqrt{2} \sin \frac{\varepsilon}{2} \quad . \tag{2.12}$$

Expanding the sine functions and keeping only the terms of first order in ε gives

$$\Delta V_{2B}(\varepsilon) = \Delta V_{1B} - \left[\frac{V_c}{\Delta V_{1B}} \sqrt{\frac{p}{R_c}} \sin P - \frac{1}{\sqrt{2}} \right] \varepsilon \quad . \tag{2.13}$$

Inserting typical Apollo values for E, R_p, and R_c, and using Equation (2.9) for ΔV_{1B}, the bracketed factor is found to be positive only for P in the range 18° to 107°. This implies two results:

$$\Delta V_{2B}(\varepsilon) \leq \Delta V_{1B} \text{ if } (18° < P < 107°) \tag{2.14}$$

$$\Delta V_{2B}(\varepsilon) \geq \Delta V_{1B} \text{ if } (0° \leq P < 18°) \text{ or } (107° < P \leq 180°) \quad , \tag{2.15}$$

the equalities holding for $\varepsilon = 0$.

The first result says that if $N_1 = 0$ and P lies in the range* 18° to 107°, then the two-burn deboost with T_1 slightly smaller than P will improve on the one-burn deboost. Therefore the optimum two-burn deboost must be a still better improvement on the one-burn deboost.

The second result says that if $N_1 = 0$ and P lies outside the range* 18° to 107°, then the two-burn deboost must degenerate to a one-burn deboost if it is to be truly optimum. The optimum in question, however is a local one, and the foregoing mathematics does not preclude the existence of another local optimum, for which the two-burn geometry would not be degenerate.**

The preceeding discussion assumed $N_1 = 0$ and compared the one- and the two-burn deboost. Can a comparison be made for those two-burn deboosts with $N_1 \neq 0$? Yes, if one considers Apollo-type missions which consist of earth launch on a specified date, flight to the moon, and lunar landing at a specified site, with all intermediate operations performed according to a standard plan. Optimization of such a mission may be regarded as variation of all trajectory parameters until a trajectory is found which satisfies the mission constraints and which requires less fuel than any other possible trajectory. If one considers optimizing a mission with a one-burn deboost and then optimizing the same mission with a two-burn deboost, one may conclude that the two-burn mission will not require more fuel than the one-burn mission. This is because the former offers more optimization variables than the latter and also includes the latter as a special case.

Thus, changing over from a deboost geometry optimization to a mission optimization allows one to compare qualitatively one- and two-burn missions which are not degenerate. The comparison cannot be made analytically because one does not know how to optimize a one-burn (Apollo-type) mission analytically.

---

*The stated range has been computed for typical Apollo values for E, R_p, R_c.

**A better optimum has not occurred for any applications of the two-burn model to Apollo simulations. In these applications, whenever the conditions $N_1 \approx 0$ and $P \ll 18°$ have occurred, the optimum two-burn deboost has degenerated to approximately a one-burn deboost.

3.0 RESULTS OF TWO-BURN SIMULATIONS

The two-burn mode of deboost may be put into perspective relative to the one-burn mode by a comparison of the effects of the two on lunar accessibility. Such a comparison will be made in this section. However, it must be pointed out that the data herein are only intended to show qualitative features of the two-burn strategy and are not the results of a comprehensive study.

The lunar mission simulations which yielded the data in this section were computed by a modified version of the Bellcomm Apollo Simulation Program. The modifications were made as required by the theory of Section 2.0 to include two-burn lunar deboosts in the mission profile. The resulting program, called DBST, operates only in the domain of patched conic, free-return trajectories. It will be described in a future memorandum.

3.1 Accessibility Filaments

A convenient way of presenting accessibility behavior is to plot Service Module fuel costs for an Apollo mission against landing site latitude, for a fixed selenographic longitude. The resulting curve will be referred to as an accessibility filament, since for a specified fuel budget it gives the location on the given longitude of the boundary of the accessible lunar surface.

Figure 3.1 shows one- and two-burn accessibility filaments for a lunar longitude of -1.0°. The missions represented simulated a launch date of October 29, 1968, and a Lunar Module plane change during ascent.* For each latitude, one can read on the abscissa the number of pounds of Service Module fuel required to fly an Apollo mission there. It is clear from the figure that, given a fuel budget, the two-burn deboost opens up the accessible lunar area relative to the one-burn deboost. In addition it is to be observed that, for this launch date, there is a rather sizable fuel saving (or payload increase) for certain sites within the Apollo zone. These observations are in agreement with the results of Reference 2.

---

*The weights and stay-times used in all the simulations in this chapter are as follows: injected spacecraft less LM adapter, 94,200 lb.; LM, 32,000 lb.; astronauts, 600 lb.; nominal stay time, 22 hr.; maximum stay time, 38 hr. All simulations herein use free-return trajectories. Mid-course corrections are not included.

An anomaly exists, however, in the crossing of the two curves of Figure 3.1. On the basis of the theory developed in Section 2, no point of the two-burn curve may lie inside the one-burn curve, because at such points the amount of fuel required for the complete one-burn mission would be less than that required for the two-burn mission. This is impossible by virtue of the two-burn optimization. Therefore the curves should at most be tangent, in which case the two-burn geometry will have reduced to the one-burn geometry. The crossing therefore indicates that the two-burn deboost is not being fully optimized by the DBST.

The problem appears to be due entirely to a scheme error resulting from the use of a one-burn optimization procedure (subroutine OPTINJ) in retargeting the hyperbola from which a two-burn deboost is made.* This difficulty is being corrected by rewriting subroutine OPTINJ. Although the error's presence probably has no important effect in most applications: it results in uncertainties which always bias the two-burn lunar mission's total fuel cost above optimum.

The data for Figure 3.1, as well as relevant geometrical data, are tabulated in Table 3.1. The table shows the important result that sites which are inaccessible with a one-burn deboost, due to the periselene depression constraint alone, are rendered accessible with the two-burn deboost.**

---

*DBST attempts to determine, after finding a free-return hyperbola and simulating a deboost from it, whether or not a more nearly optimum free-return hyperbola exists, in the sense of smaller lunar deboost delta velocity. This is done by an optimization procedure in the subroutine OPTINJ. Since the criterion for improvement is the deboost delta velocity, this optimization procedure clearly depends on the deboost strategy. It therefore must be different for one- and two-burn deboosts.

**For a one-burn deboost to be possible, a hyperbola must be chosen which intercepts the desired parking orbit. It sometimes happens, due to the free-return constraint, that this cannot be achieved without lowering the periselene altitude below a specified minimum (say, forty nautical miles) in which case the site in question would be deemed inaccessible. Using the two-burn strategy, however, no site need be made inaccessible for this reason, since the hyperbola now need not be forced to intersect the parking orbit.

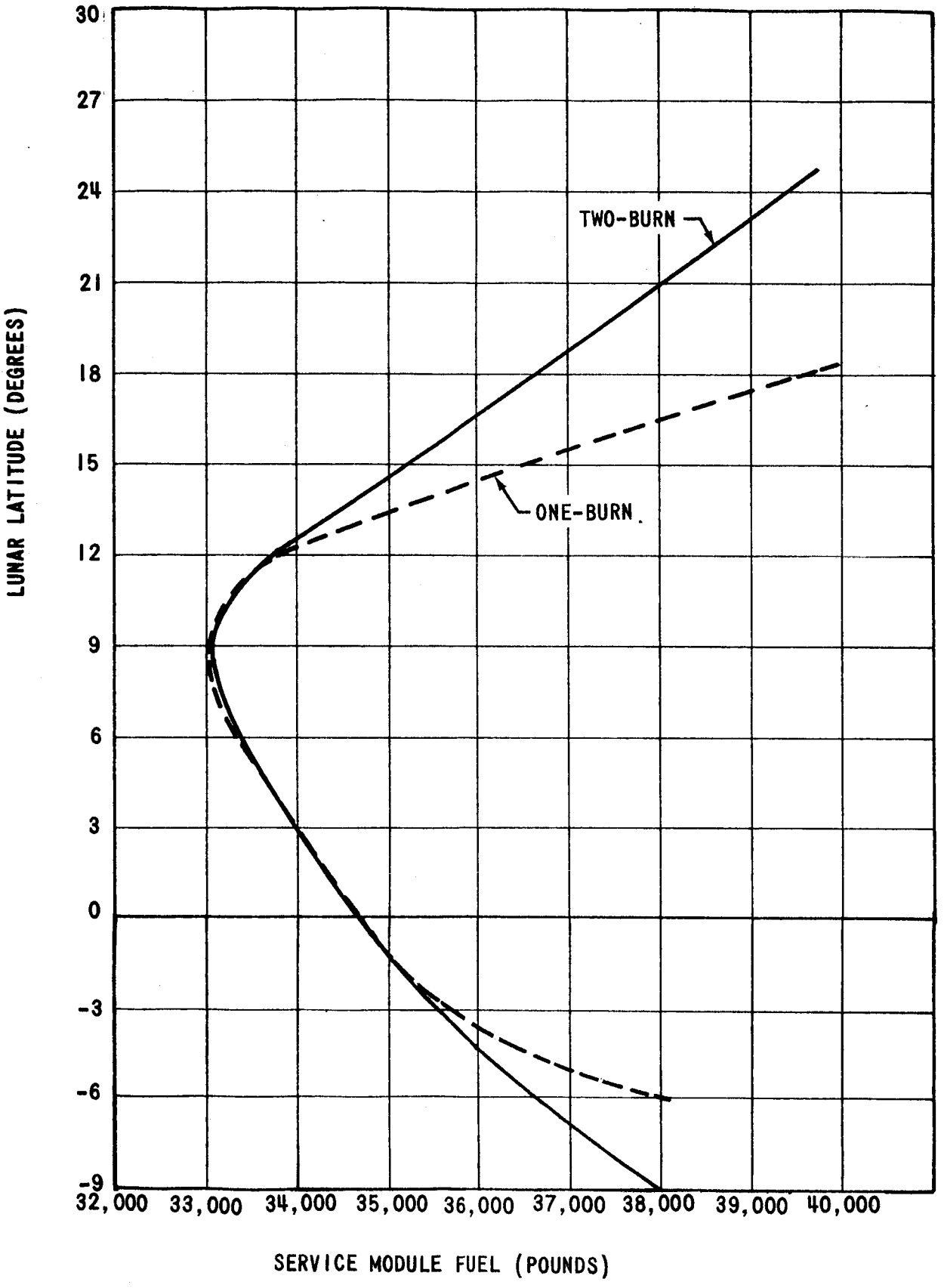

FIGURE 3.1 - ACCESSIBILITY FILAMENTS AT 1.0° WEST LONGITUDE FOR LAUNCH DATE OCTOBER 29, 1968 (LUNAR MODULE PLANE CHANGE)

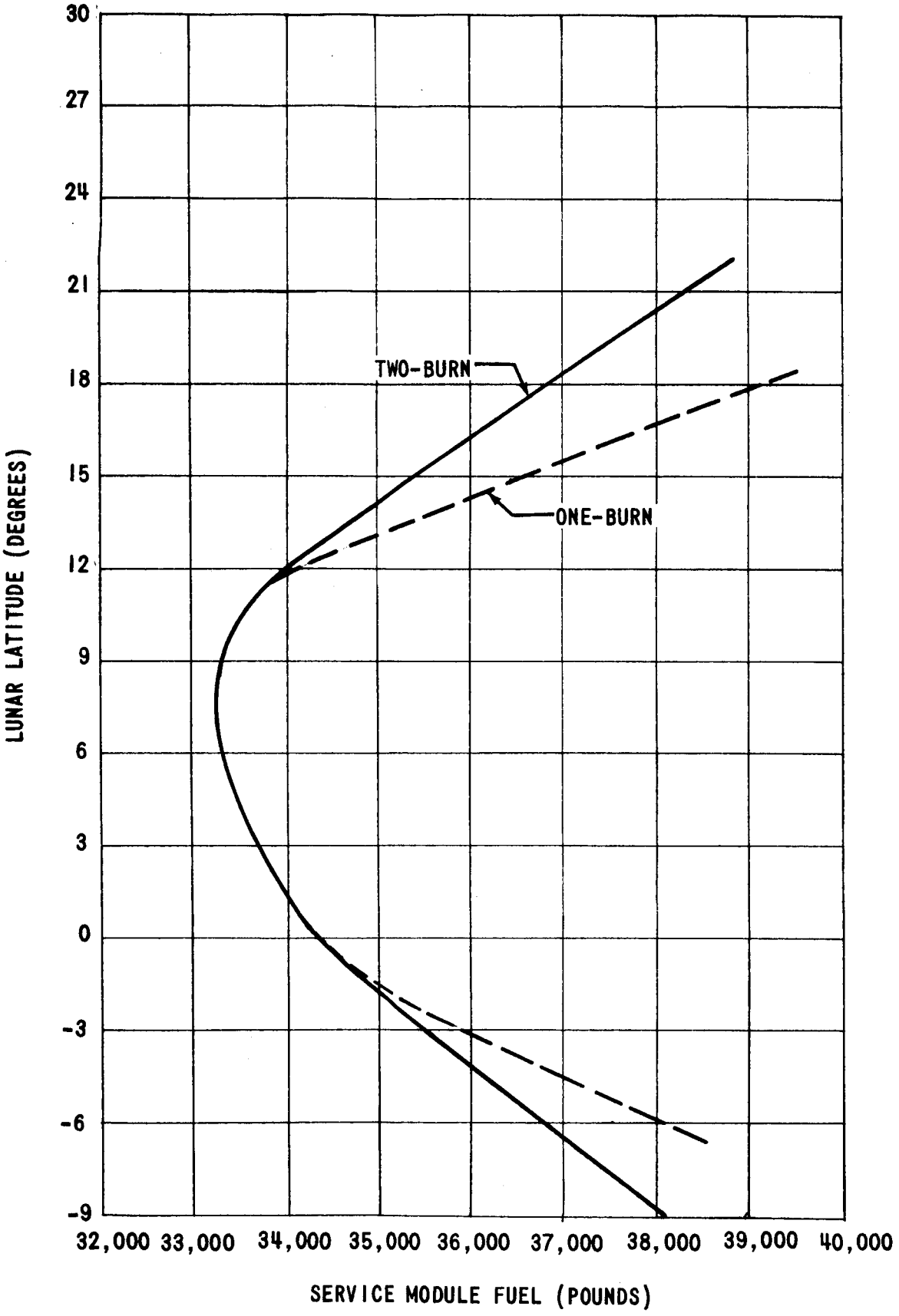

FIGURE 3.2 - ACCESSIBILITY FILAMENTS AT 1.0° WEST LONGITUDE FOR LAUNCH DATE OCTOBER 29, 1968 (COMMAND MODULE PLANE CHANGE)

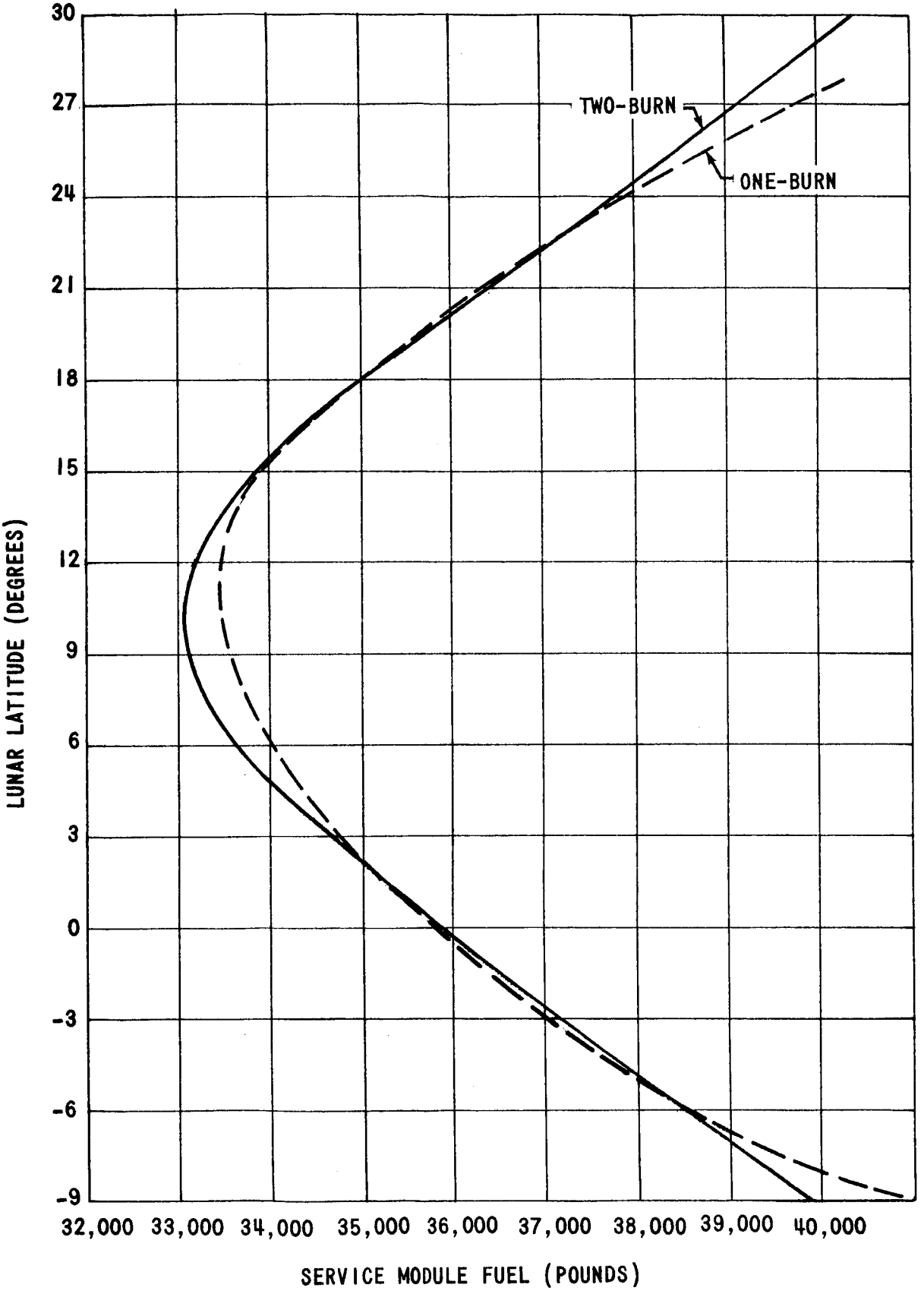

FIGURE 3.3 - ACCESSIBILITY FILAMENTS AT 30.0° WEST LONGITUDE FOR LAUNCH DATE OCTOBER 29, 1968 (COMMAND MODULE PLANE CHANGE)

TABLE 3.2

DATA FOR ACCESSIBILITY FILAMENTS AT 1.0° WEST LONGITUDE
FOR LAUNCH DATE OCTOBER 29, 1968 (COMMAND MODULE PLANE CHANGE)

	Latitude (deg)	Fuel (lbs)	Az* (deg)	P (deg)	F (deg)	N1 (deg)	Periselene Depression (ft)
TWO-BURN	-9.0	38097	-78	9.39	-63.069	-59.367	7,767
	-6.0	36832	-78	7.04	-50.203	-45.917	10,417
	-3.0	35536	-78	5.28	-27.635	-23.397	10,194
	0.0	34349	-76	2.26	- 1.482	- 1.342	11
	3.0	33642	-76	0.11	-115.348	-115.348	0
	6.0	33300	-82	4.30	2.134	0.013	2,510
	9.0	33272	-84	4.06	4.411	0.239	9,723
	12.0	34001	-84	1.30	23.159	23.159	0
	15.0	35384	-84	3.61	-108.974	-108.974	0
	18.0	36759	-84	6.51	-100.959	-102.886	2,091
	21.0	38226	-84	10.95	40.799	33.393	30,836
ONE-BURN	-9.0	42097	-98	26.01	-19.621	. . . .	230,211
	-6.0	38084	-90	17.63	-19.056	. . . .	216,725
	-3.0	35896	-84	11.08	-14.251	. . . .	119,847
	0.0	34308	-78	4.32	- 4.564	. . . .	11,853
	3.0	. . . . .	TIME OF	FLIGHT	DIFFICULTY	. . . . .	. . . . .
	6.0	33298	-82	4.29	2.137	. . . .	25,291
	9.0	33271	-84	4.06	4.447	. . . .	10,844
	12.0	34115	-86	3.26	8.709	. . . .	41,151
	15.0	36592	-92	9.73	20.394	. . . .	217,180
	18.0	39087	-66	18.16	-19.310	. . . .	220,749

* Flight path azimuth at landing of Lunar Module.

** This equals 80 NM minus the periselene altitude.

TABLE 3.3

DATA FOR ACCESSIBILITY FILAMENTS AT 30.0° WEST, LONGITUDE FOR LAUNCH DATE OCTOBER 29, 1968 (COMMAND MODULE PLANE CHANGE)

	Latitude (deg)	Fuel (lbs)	Az* (deg)	P (deg)	F (deg)	N1 (deg)	Periselene Depression** (ft)
TWO-BURN	-9.0	39865	-86	19.77	-30.107	-13.973	146,466
	-6.0	38492	-86	17.39	-24.249	- 8.369	141,990
	-3.0	37105	-86	15.21	-15.767	- 1.493	131,519
	0.0	35901	-86	13.33	- 7.088	- 0.047	28,055
	3.0	34689	-90	12.82	- 5.738	- 0.009	18,334
	6.0	33607	-86	7.76	- 1.840	0.222	2,376
	9.0	33127	-86	4.49	1.937	0.519	1,123
	12.0	33138	-86	0.95	21.933	20.038	2,006
	15.0	33917	-86	2.99	-10.123	- 7.429	4,078
	18.0	35021	-84	6.97	-13.807	- 7.120	25,154
	21.0	36462	-82	10.48	-19.146	- 9.265	54,817
	24.0	37844	-82	12.79	-28.465	-17.914	62,477
	27.0	39171	-84	14.51	-41.831	-32.822	45,601
	30.0	40490	-86	16.84	-51.984	-44.136	34,616
ONE-BURN	- 9.0	40172	-90	22.27	-20.097	. . . .	241,643
	- 6.0	38514	-88	18.77	-18.588	. . . .	206,033
	- 3.0	37101	-86	15.26	-16.400	. . . .	159,582
	0.0	35815	-86	13.34	- 7.277	. . . .	30,712
	3.0	34776	-84	9.74	- 3.944	. . . .	8,868
	6.0	34034	-84	6.70	- 1.685	. . . .	1,594
	9.0	33560	-86	4.43	1.218	. . . .	821
	12.0	33500	-90	2.71	6.619	. . . .	23,856
	15.0	33899	-86	3.14	- 7.209	. . . .	29,621
	18.0	35011	-84	7.17	-11.318	. . . .	74,290
	21.0	36413	-80	12.12	-10.134	. . . .	59,447
	24.0	37996	-80	17.18	-19.451	. . . .	223,884
	27.0	39759	-76	18.98	-16.238	. . . .	155,007
	30.0	41475	-74	22.41	-17.649	. . . .	183,709

* Flight path azimuth at landing of Lunar Module.

** This equals 80 NM minus the periselene altitude.

TABLE 3.4

COMPARISON OF ONE- AND TWO-BURN MISSIONS

TO SEVERAL ORBITER SITES

ORBITER SITE		LAUNCH DATE	TOTAL MISSION FUEL COST (pounds)*	
Latitude	Longitude	(1968)	Lunar Module Plane Change	Command Module Plane Change
4.30°	21.30°	May 1	32796 **	33056 33102
4.75°	15.75°	May 1	33383 **	33315 33311
0.75°	24.17°	Dec.22	34357 34407	33904 33919
-0.08°	- 1.00°	Oct.26	35343 35728	35547 35911
1.50°	-42.33°	Oct. 29	35381 35390	35205 35558
-2.35°	-43.37°	Sept.30	37683 37658	37717 37691

* Upper figures are two-burn; lower are one-burn.

** Periselene depression constraint exceeded; site inaccessible on this date.

For the sake of comparison, Figure 3.2 gives one-and two-burn accessibility filaments at the same longitude and on the same launch date as for Figure 3.1, but with the Service Module making the plane change prior to rendezvous with the Lunar Module. Table 3.2 gives the relevant geometrical data. Although the orientations of the curves are seen to have changed, the observations are substantially the same as for Figure 3.1.

Figure 3.3 gives another accessibility filament, at -30.0° longitude, for the same launch date and for a Service Module plane change. The geometrical data are in Table 3.3. The figure is similar to the previous two, in that the one-burn curve nests tightly into the two-burn curve. It is different in that the two-burn filament offers sizable fuel savings over the one-burn filament at sites near that latitude about which the filaments are approximately symmetrical.

Since during a month the accessibility filaments must reflect the moon's librations, one may expect the maximum fuel savings to scan various latitudes that are within the Apollo zone,* in a periodic fashion. One also expects libration effects on the other accessibility filaments of this section, of course.

Another difference is to be found between Figure 3.3 and Figures 3.1 and 3.2. It is that for small longitudes (longitudes rather near the lunar prime meridian) the two-burn deboost begins to improve on one-burn accessibility at "lower" latitudes, while for large longitudes the improvement begins at "higher" latitudes.

This concludes the analysis of the sample accessibility filaments themselves. Looking now a little more broadly at the results of the two-burn simulations, one might speculate that the two-burn model contains a heretofore unexpected advantage over Apollo's present one-burn scheme. The advantage is this: The optimum periselene radius is found to settle itself very close (within about five miles) to the parking orbit radius, which has been chosen to be 80 NM plus the lunar radius. If this feature persists for smaller parking orbit altitudes, then one might use it to decrease Lunar Module performance requirements, by lowering the periselene and parking orbit radii in the mission profile.**

---

*The Apollo zone is the area of the lunar surface which is bounded by ± 45° longitude and ± 5° latitude.

**Implications of lowering parking orbit altitude are discussed in a memorandum by D. R. Valley (Reference 5).

3.2 Data for Selected Sites

Table 3.4 presents fuel costs for missions flown to several selected sites in the Apollo zone* on days when the one-burn fuel cost is known to be high. The principal observation to be made, after noting the presence of DBST's scheme error, is that the two-burn strategy provides reasonable fuel savings (about 300 pounds) in only a fraction of the cases presented. However, it is to be expected that the effectiveness of the two-burn strategy in getting to any particular landing site will vary with launch date. This is because of the effect identified in Section 3.1, namely, that the greatest fuel saving along a lunar longitude will occur at a latitude which is a function of the lunar librations. Consequently, in the absence of simulation data for many sites and many launch dates, no general comments are possible on the efficacy of the two burn strategy applied to specific sites.

---

*The sites were chosen from a set photographed by Lunar Orbiters I and II.

4.0 SUMMARY AND CONCLUSIONS

In Section 2.0 a two-burn model for deboosting from a hyperbola into a specified circular parking orbit, via an intermediate circular orbit, was described and developed analytically. This yielded a formula for the two-burn deboost delta velocity and, as a side result, a formula for the one-burn delta velocity. It was shown how the model's deboost delta velocity may be optimized with respect to two variables.

The analysis of the two-burn model has been incorporated into the conic portion of BCMASP, replacing BCMASP's (free-return) one-burn lunar deboost simulation. The resulting conic program, called DBST, has been used as a means of studying the efficacy for Apollo of this particular two-burn deboost strategy. The results of the study are the following:

1. The two-burn strategy increases the accessible area of the lunar surface relative to that which is accessible with Apollo's present one-burn strategy.

2. With regard to periselene limits alone, no site is inaccessible with a two-burn deboost. Two-burn accessibility is therefore limited exclusively by fuel capability, contrary to the case for one-burn accessibility.

3. The optimum periselene for two-burn deboosts is found to lie near the parking orbit for the simulations studied, all of which had 80 NM parking orbits. If this feature persists for smaller parking orbit altitudes, then one might use it to reduce Lunar Module performance requirements, by lowering the periselene and parking orbit radii in the mission profile.

4. The two-burn deboost offers, relative to the one-burn deboost, total mission fuel savings on the order of 300 or 400 pounds, for missions flown to selected Apollo landing sites. Still greater savings are possible for sites with latitudes outside the Apollo range of $\pm 5°$. However, the saving associated with a particular site will vary with time, due to lunar librations.

A comparison of the fuel savings reported herein with those known to be available with more general two-burn deboosting schemes (see References 1 and 6, for example) shows that there are definite advantages to optimum two-burn targeting schemes which allow the first burn to occur at or near the moon's sphere of influence. Study of such schemes is planned as part of a continuing effort in the design of practical, as well as optimum, multiple-impulse deboost schemes and their associated targeting programs.

S. L. Levie, Jr.

2011-SLL-jdc S. L. Levie, Jr.

ACKNOWLEDGMENTS

The author wishes to thank William D. Kinney for several educational discussions on the subject of BCMASP. Special thanks are due Elizabeth A. Carty, who did the programming which resulted in DBST, including a great deal of backup work.

REFERENCES

1. Gunther, P., "Optimum Two-Impulse Deboost into Lunar Orbit." Bellcomm Technical Memorandum, March 31, 1965.

2. Dudek, J. S., "A Generalized Two-Burn Deboost Technique which Increases Apollo Lunar Accessibility - Case 310," Bellcomm Memorandum for File, June 23, 1966.

3. Dudek, J. S., "Lunar Accessibility for April - May 1968 Using Two Burn Lunar Deboost - Case 310," Bellcomm Memorandum for File, December 2, 1966.

4. Amman, R. J., Mission Analysis and Open-Loop Trajectory Targeting Theory for the Bellcomm Apollo Simulation Program. Bell Telephone Laboratories; January 10, 1966.

5. Valley, D. R., "Implications of Lower Lunar Orbital Altitudes for LM Separation," Bellcomm Technical Memorandum, August 1, 1967.

6. O'Malley, J. P., et al, "Site Accessibility Analysis for Advanced Lunar Missions, MSC/TRW Task A-89", TRW Note No. 67-FMT-517, June 30, 1967.

APPENDIX I: SOME PROPERTIES OF A HYPERBOLA

In its own plane, a hyperbola's shape and configuration relative to the center of attraction, or occupied focus, are commonly given by the two geometrical parameters a and e, respectively the semimajor axis and the eccentricity. In what follows several quantities for a hyperbola will be derived, including a and e, in terms of two kinematic parameters: the energy E and the distance R_p from the focus to pericenter.

A relation that is presented in the usual discussions of hyperbolas is

$$V^2 = GM \left(\frac{2}{R} + \frac{1}{a}\right) , \qquad (I.1)$$

in which R and V are the position and velocity of a point on the hyperbola and GM is the gravitational constant times the mass of the attracting body. If we use the specific energy

$$E = \frac{1}{2} V^2 - \frac{GM}{R} \qquad (I.2)$$

at the same point, then a can be solved for in terms of E:

$$a = GM/2E. \qquad (I.3)$$

With this in hand, we may substitute a in the fundamental conic formula $R_p = a(e-1)$ and solve for e:

$$e = 1 + 2R_pE/GM \qquad (I.4)$$

We now can also rewrite the standard formula for the parameter p of the hyperbola:

$$p = a(e^2 - 1) = 2R_p \left(\frac{ER_p}{GM} + 1\right) . \qquad (I.5)$$

APPENDIX I - (continued)

Let us derive an expression for the true anomaly of an arbitrary point on the hyperbola. The point will be specified by its distance R_c from the focus. [Obviously there are no such points if $R_c < R_p$, and there are two such points if $R_c > R_p$.]

The polar equation of a hyperbolic orbit is

$$R = \frac{p}{1 + e \cos \phi},$$

in which ϕ is the true anomaly of the point at distance R. Setting $R = R_c$ and substituting Equation (1.5) for e leads to

$$\cos \phi = \frac{\frac{p}{R_c} - 1}{\frac{p}{R_p} - 1} . \qquad (1.6)$$

Notice that ϕ has an ambiguous sign, as expected, and that it is a function only of E, R_p, and R_c (see Equation (I.4)).

We now conclude by presenting the radial and perpendicular components of the velocity $\vec{V}$ at a point $\vec{R}_c$ on a hyperbola. These components are respectively parallel and perpendicular to $\vec{R}_c$ and will be labeled by $\vec{V}_R$ and $\vec{V}_H$.

Notice that if α is the angle between $\vec{R}_c$ and $\vec{V}$, then $V_H = V \sin \alpha$. The specific angular momentum, defined as $h = |\vec{R}_c \times \vec{V}|$, is therefore

$$h = R_c V_H .$$

But, as the standard texts show,

APPENDIX I -(continued)

$$h = \sqrt{pGM} .$$

Hence

$$V_H = \frac{\sqrt{pGM}}{R_c} \tag{I.7}$$

Since $\sqrt{GM/R_c}$ is the velocity V_c of a mass in circular orbit of radius R_c about the center of attraction, this can be rewritten as

$$V_H = V_c \sqrt{\frac{p}{R_c}} . \tag{I.8}$$

Using the fact that $\vec{V}_H$ and $\vec{V}_R$ are perpendicular and observing that Equation (I.1) can be rewritten as

$$V^2 = 2V_c^2 + 2E,$$

we can readily obtain V_R^2:

$$\begin{aligned} V_R^2 &= V^2 - V_H^2 \\ &= 2V_c^2 + 2E - V_c^2 \frac{p}{R_c} \\ &= V_c^2 \left(2 + \frac{2R_cE}{GM} - \frac{p}{R_c} \right). \end{aligned} \tag{I.9}$$

APPENDIX II: THE T_1 OPTIMIZATION

In Section 2.0 an expression was derived for the two-burn delta velocity, ΔV_{2B}. Regarding ΔV_{2B} as a function of T_1 alone, it will be determined in this appendix how to compute that T_1 which minimizes ΔV_{2B}.

II.1 Choice of D

To begin, it must be determined which value of D to use in ΔV_{2B} (Section 2.3). A cursory inspection of the formula reveals that the optimum choice of D depends on the values of the parameters P, F, and $\arccos\left(\frac{p/R_c - 1}{p/R_p - 1}\right)$ and also on the quadrant of the optimum T_1, which, however, is specified by the three parameters. The theorem for D could be constructed at this point, but, although the procedure is straightforward, the mathematics is too complicated to present here with useful returns. Instead, the problem will be solved by a qualitative argument.

To simplify matters, the realistic conditions $0° < P < 90°$ and $|F| < 90°$ will be imposed. For hyperbolas which pierce the reference plane twice, the pierce point toward which F is to be measured should be chosen accordingly.

Consider the spherical projection in Figure II.1, which shows an approach hyperbola and the plane of the final circle. The dot locates pericenter ($0° < F < 90°$), and the numbered crosses locate the two possible transfer points. The goal is to determine whether transferring from (1) in the optimum two-transfer maneuver will be more, or less, optimum than transferring from (2). Because of the different elevations of the two candidates, the lower one allows the possibility of a smaller T_2 than the upper, simply because of the spherical relations involved. Since the

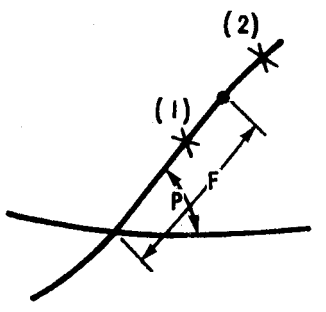

Figure II.1 - Choosing D

optimization process must to some extent minimize T_2, it should be to our advantage to transfer from the point which is closer to the reference plane--point (1) in this case. Notice that for this configuration it is also obvious that T_1 must be positive.

Now consider Figure II.2 which shows a hyperbola such that $-90° < F < 0°$. By the same argument, one now should transfer at point (2), which is closer to the reference plane than is point (1). T_1 will again be positive.

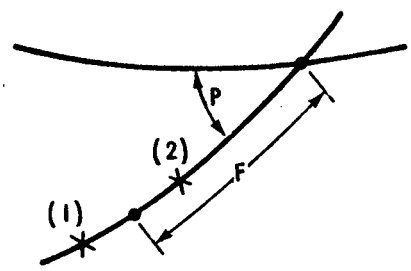

Figure II.2 - Choosing D

For both these cases, it is seen from the figures that N_1 is smaller in magnitude that F, so for D one should choose

$$D = \text{sign}(F) \tag{II.1}$$

in order for the calculation of N_1 to reproduce this fact. This result can be shown analytically along with the related generalizations, one of which is that if $|F| > 90°$ then one should take $D = -\text{sign}(F)$.

II.2 Optimization with Respect to T_1

With D determined, one is in a position to optimize V_{2B} with respect to T_1, which will be done by forming the derivative $d(\Delta V_{2B})/dT_1$, and setting it equal to zero. When all simplifications are made in the resulting equation, a sixth degree polynomial in tan T_1 obtains. This is presented in Equation (II.10), Figure II.4. Thus optimizin ΔV_{2B} with respect to T_1 requires solving a sixth degree polynomial, which must be done numerically, in general. The remainder of this appendix will be devoted to this polynomial.

The two-burn delta velocity may be written as

Appendix II

$$\Delta V_{2B} = \sqrt{\frac{2GM}{R_c}}\left\{\left(\frac{3}{2} + \frac{ER_c}{GM} - \sqrt{\frac{p}{R_c}}\cos T_1\right)^{\frac{1}{2}} + (1-\cos T_1 \cos P - \sin T_1 \sin P \cos N_1)^{\frac{1}{2}}\right\}. \qquad \text{(II.2)}$$

Differentiating with respect to T_1 and setting the derivative to zero gives

$$0 = \frac{\sqrt{\frac{p}{R_c}}\sin T_1}{\left(\frac{3}{2} + \frac{ER_c}{GM} - \sqrt{\frac{p}{R_c}}\cos T_1\right)^{\frac{1}{2}}} + \frac{\cos P \cos T_1 - \sin P \cos N_1 \cos T_1}{(1-\cos T_1 \cos P - \sin T_1 \sin P \cos N_1)^{\frac{1}{2}}} \qquad \text{(II.3)}$$

To simplify the expressions, the following definitions are introduced:

$$\left.\begin{aligned} s &= \sqrt{\frac{R_p}{R_c}} \\ g &= \frac{3}{2} + \frac{R_c E}{GM} \\ e &= \cos P \\ f &= \sin P \cos N_1 . \end{aligned}\right\} \qquad \text{(II.4)}$$

Appendix II (contd.)

These simplify (II.3) to

$$0 = \frac{s \sin T_1}{(g - s \cos T_1)^{\frac{1}{2}}} + \frac{e \sin T_1 - f \cos T_1}{(1 - e \cos T_1 - f \sin T_1)^{\frac{1}{2}}}$$

Now square this, divide the numerators by $\cos^2 T_1$, divide the denominators by $\cos T_1$, and use the identity $(\cos T_1)^{-1} = (1 + \tan^2 T_1)^{1/2}$. The net result is

$$\frac{(e \tan T_1 - f)^2}{(1 + \tan^2 T_1)^{\frac{1}{2}} - e - f \tan T_1} = \frac{s^2 \tan^2 T_1}{g(1 + \tan^2 T_1)^{\frac{1}{2}} - s} \qquad \text{(II.5)}$$

The zero derivative, Equation (II.3), has been converted to this function of tangents, in preference to a function of sines or cosines, principally to insure that the roots of the function will be well separated in magnitude. Thus the necessity of using numerical methods is anticipated.

Equation (II.5) must now be manipulated so that the radical can be squared away. Squaring both sides and rearranging the result gives

$$(1 + \tan^2 T_1)^{\frac{1}{2}} [g(e \tan T_1 - f)^2 - s^2 \tan^2 T_1]$$

$$= [s(e \tan T_1 - f)^2 - es^2 \tan^2 T_1 - fs^2 \tan^3 T_1] \; . \qquad \text{(II.6)}$$

The left side, which is now defined to be $(1 + \tan^2 T_1)^{\frac{1}{2}} H$, and the right side, defined to be N, will be squared and simplified separately, and then combined to give the final polynomial,

Appendix II (contd.)

$(1 + \tan^2 T_1)H^2 - N^2 = 0$. These calculations are shown explicitly on the following pages in Figures II.3 and II.4, the polynomial itself appearing Equation (II.10).

It should be observed that the polynomial has roots that are extraneous to the problem since we have squared twice, and also that that root tan T_1 which actually corresponds to a minimum in ΔV_{2B} does not uniquely specify the optimum angle T_1 in the domain -180° to 180°. Therefore, to use the polynomial one must:

(i) numerically solve Equation (II.10) for its six roots tan T_1

(ii) for each of the real roots find the two corresponding angles T_1

(iii) substitute all resulting T_1's into Equation (II.2) to find out which one minimizes ΔV_{2B}.

II.3 Example Solution

It is of interest to compare a graphically determined minimum of ΔV_{2B} with the minimum produced by solving the optimization polynomial (II.10).

A plot of ΔV_{2B} versus T_1 is presented in Figure II.5, for which the parameters

$P = 4.776697°$

$F = -3.110090°$

$R_p = 6{,}185{,}166.4$ ft.

$R_c = 6{,}188{,}483.0$ ft.

$E = 6{,}086{,}558.7$ ft^2/sec^2

$GM = 1.7313996 \times 10^{14}$ ft^3/sec^2

Appendix II (Contd.)

were used. These correspond to typical Apollo lunar approach parameters. The plot is observed to have the optimum values

$$\left.\begin{aligned} T_{1,\ \text{optimum}} &= 4.75^\circ \pm 0.05^\circ \\ \Delta V_{2B,\ \text{optimum}} &= (3025 \pm 2)\ \text{ft/sec} \end{aligned}\right\}\ \text{graphical.}$$

For the same parameter values, a computer solution of Equation (II.10) produced the result

$$\left.\begin{aligned} T_{1,\ \text{optimum}} &= 4.76360^\circ \\ \Delta V_{2B,\ \text{optimum}} &= (3024.93)\ \text{ft/sec} \end{aligned}\right\}\ \text{semi-analytic.}$$

The agreement between these two sets verifies the correctness of Equation (II.10).

$$H \equiv g(e \tan T_1 - f)^2 - s^2 \tan^2 T_1 = (ge^2-s^2)\tan^2 T_1 - 2gef \tan T_1 + gf^2$$

$$H^2 = (ge^2-s^2)^2 \tan^4 T_1 - 4gef(ge^2-s^2)\tan^3 T_1 + 2gf^2(3ge^2-s^2)\tan^2 T_1$$

$$- 4g^2ef^3 \tan T_1 + g^2f^4 \qquad \text{(II.7)}$$

$$\begin{aligned}(1 + \tan^2 T_1)H^2 &= (ge^2-s^2)\tan^6 T_1 - 4gef(ge^2-s^2)\tan^5 T_1 \\ &+ [2gf^2(3ge^2-s^2) + (ge^2-s^2)^2]\tan^4 T_1 - 4gef[ge^2-s^2 + gf^2]\tan^3 T_1 \\ &+ gf^2[6ge^2-2s^2 + gf^2]\tan^2 T_1 - 4g^2ef^3 \tan T_1 + g^2f^4 \\ &= [g^2e^4 - 2ge^2s^2 + s^4]\tan^6 T_1 + [4gefs^2 - 4g^2e^3f]\tan^5 T_1 \\ &+ [6g^2e^2f^2 - 2gf^2s^2 + g^2e^4 - 2ge^2s^2 + s^4]\tan^4 T_1 \\ &+ [4gefs^2 - 4g^2e^3f - 4g^2ef^3]\tan^3 T_1 + [6g^2e^2f^2 - 2gf^2s^2 + g^2f^4]\tan^2 T_1 \\ &- 4g^2ef^3 \tan T_1 + g^2f^4 \qquad \text{(II.8)}\end{aligned}$$

FIGURE II.3 - Computation of H, H^2, and $(1 + \tan^2 T_1)H^2$

$$N \equiv s(e \tan T_1 - f)^2 - s^2 f \tan^3 T_1 - es^2 \tan^2 T_1$$

$$= -f s^2 \tan^3 T_1 + es(e-s)\tan^2 T_1 - 2efs \tan T_1 + f^2 s$$

$$N^2 = f^2 s^4 \tan^6 T_1 + [2efs^4 - 2e^2 fs^3]\tan^5 T_1 + [e^4 s^2 + e^2 s^4 - 2e^3 s^3 + 4ef^2 s^3]\tan^4 T_1$$

$$+ [4e^2 fs^3 - 2f^3 s^3 - 4e^3 fs^2]\tan^3 T_1 + [6e^2 f^2 s^2 - 2ef^2 s^3]\tan^2 T_1$$

$$- 4ef^3 s^2 \tan T_1 + f^4 s^2 \qquad \text{(II.9)}$$

$$0 = (1+\tan^2 T_1)H - N^2 = [g^2 e^4 - 2ge^2 s^2 + s^4 - f^2 s^4]\tan^6 T_1$$

$$+ [4gefs^2 - 4g^2 e^3 f + 2e^2 fs^3 - 2efs^4]\tan^5 T_1 + [2e^3 s^3 - e^4 s^2 - e^2 s^4 - 4ef^2 s^3$$

$$+ 6g^2 e^2 f^2 - 2gf^2 s^2 + g^2 e^4 - 2ge^2 s^2 + s^4]\tan^4 T_1$$

$$+ [4gefs^2 - 4g^2 e^3 f - 4g^2 ef^3 + 2f^3 s^3 + 4e^3 fs^2 - 4e^2 fs^3]\tan^3 T_1$$

$$+ [-2gf^2 s^2 + g^2 f^4 + 2ef^2 s^3]\tan^2 T_1 - 4ef^2(g^2 - s^2)\tan T_1 + f^4(g^2 - s^2) \qquad \text{(II.10)}$$

FIGURE II.4 - Computation of N, N^2, and the tan T_1 Polynomial

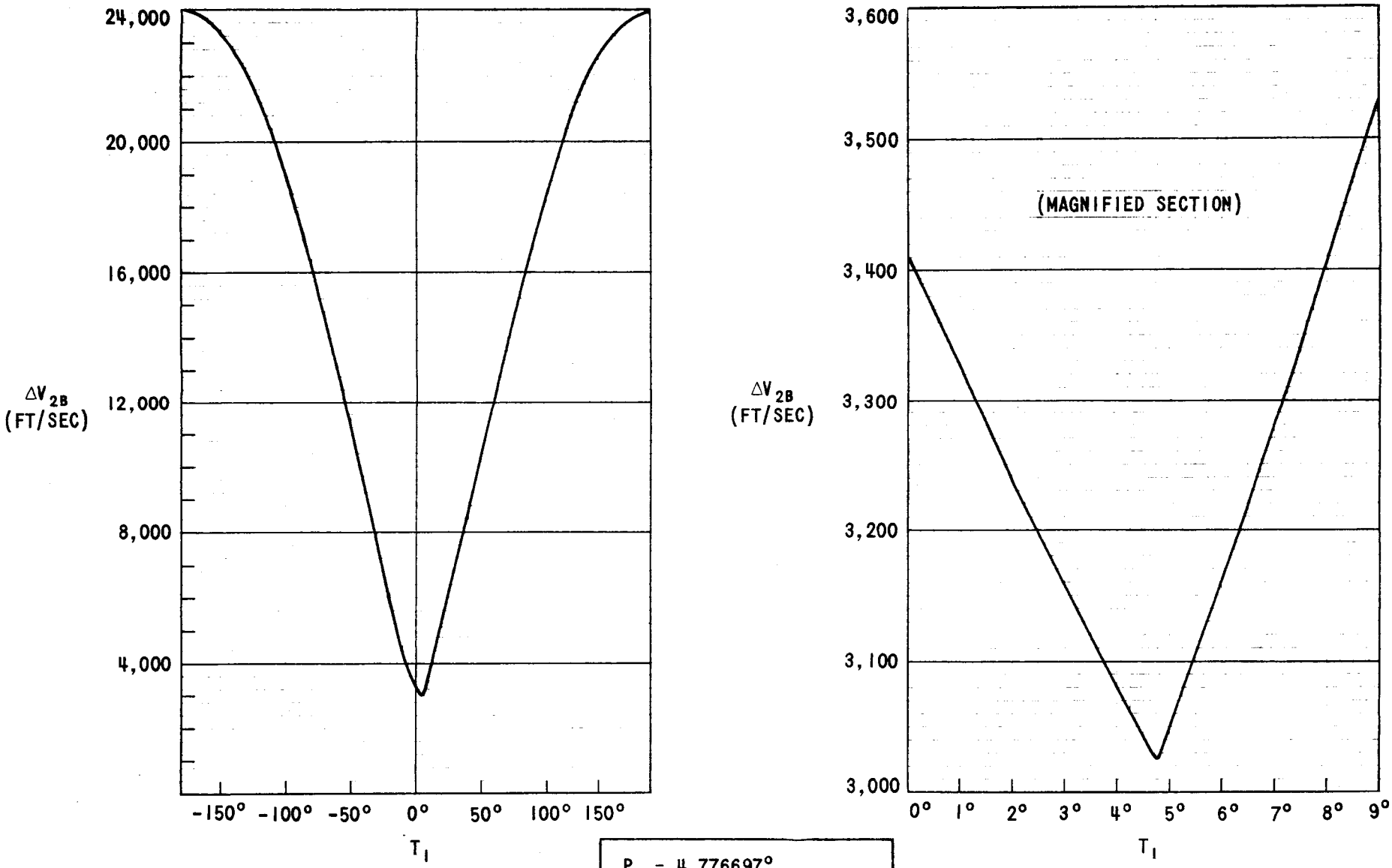

P = 4.776697°
F = -3.110090°
E = 6086558.7 FT^2/SEC^2
R_C = 6188483.06 FT
R_P = 6185166.44 FT

FIGURE 11.5 - ΔV_{2B} vs T_1